

Insights into the Structure and Dynamics of a Room-Temperature Ionic Liquid: Ab Initio Molecular Dynamics Simulation Studies of 1-*n*-Butyl-3-methylimidazolium Hexafluorophosphate ([bmim][PF₆]) and the [bmim][PF₆]-CO₂ Mixture

B. L. Bhargava[†] and S. Balasubramanian*

Chemistry and Physics of Materials Unit, Jawaharlal Nehru Centre for Advanced Scientific Research, Jakkur, Bangalore 560 064, India

Received: December 23, 2006; In Final Form: February 18, 2007

Ab initio molecular dynamics (AIMD) studies have been carried out on liquid 1-*n*-butyl-3-methylimidazolium hexafluorophosphate ([bmim][PF₆]) and its mixture with CO₂ using the Car–Parrinello molecular dynamics (CPMD) method. Results from AIMD and empirical potential molecular dynamics (MD) have been compared and were found to differ in some respects. With a strong resemblance to the crystal, the AIMD simulated neat liquid exhibits many cation–anion hydrogen bonds, a feature that is almost absent in the MD results. The anions were observed to be strongly polarized in the condensed phase. The addition of CO₂ increased the probability of this hydrogen bond formation. CO₂ molecules in the vicinity of the ions of [bmim][PF₆] exhibit larger deviations from linearity in their instantaneous configurations. The polar environment of the liquid induces a dipole moment in CO₂, lifting the degeneracy of its bending mode. The calculated splitting in the vibrational mode compares well with infrared spectroscopic data. The solvation of CO₂ in [bmim][PF₆] is primarily facilitated by the anion, as seen from the radial and spatial distribution functions. CO₂ molecules were found to be aligned tangential to the PF₆ spheres with their most probable location being the octahedral voids of the anion. The structural data obtained from AIMD simulations can serve as a benchmark to refine interaction potentials for this important room-temperature ionic liquid.

1. Introduction

The two classes of environmentally benign solvents that currently receive attention are supercritical carbon dioxide (scCO₂) and the collection of room-temperature ionic liquids (RTILs). In areas of polymer synthesis and processing, scCO₂ has been suggested as a replacement for chlorofluorocarbons (CFCs).¹ scCO₂ is one of the well-studied systems through a combination of experimental^{2,3} and computational^{4–6} approaches. It possesses liquidlike densities and gaslike transport properties. However, RTILs possess negligible vapor pressure and a wide liquid range. They can, in principle, be tailor-made for a specific application by appropriate mixing of pure components.^{7,8} Due to their properties and the potential applications, these compounds have been widely studied.^{9–19} A variety of computational methods, including simulations of RTILs, have provided a microscopic picture of these systems.^{20–29} RTILs too can have the potential to replace volatile organic solvents that are currently employed in several synthetic procedures.⁷ However, the recovery or extraction of the products of a chemical reaction that is conducted in an ionic liquid via distillation is difficult due to the low volatility of the solvent.³⁰ The possibility of redressing this limitation by using scCO₂ has attracted much recent attention.^{31–34} Furthermore, the interaction between the solute and the solvent in the mixture can impart new properties that the individual components may not possess.³⁵ The current focus of research on these mixtures is on the need to understand the molecular-level interactions between the RTIL and CO₂.^{36–42}

CO₂ is remarkably soluble in imidazolium-based ionic liquids.^{31,43–47} However, the solubility of ILs in CO₂ is immeasurably low.^{31,43} This opens up the possibility of extracting products of an organic reaction or contaminants from ionic liquids using CO₂. Brennecke and co-workers³³ have demonstrated the separation of organic compounds and water from ILs using CO₂.

The RTIL–CO₂ mixture has been studied from the viewpoint of understanding the molecular-level interactions by Maginn and co-workers.³⁸ By examination of the effect of varying the anion among different ILs, their experiments and computer simulations have shown that the anion influences the solubility of CO₂ to a larger extent than the cation. The nature of this anion–CO₂ interaction was probed using vibrational spectroscopic methods by Kazarian et al.³⁶ who found evidence of a weak Lewis acid–base interaction between CO₂ and the anions of the ILs. Analyses of the void distribution in computer-generated configurations of the IL–CO₂ mixture have shown that the CO₂ molecules are predominantly found to be located in pre-existing void spaces in the IL that reorganize to accommodate the CO₂.⁴⁰ This observation offers a neat explanation for the negligible increase in molar volume of the solution compared to that of the pure IL. In a recent X-ray diffraction study,⁴¹ Kanakubo and co-workers have examined the intermolecular structure of the solution, in particular the location and orientation of the CO₂ molecule with respect to the PF₆ anion. They concluded that the CO₂ molecule may not be tangential to the PF₆ sphere as was claimed in the computer simulation studies.^{38,40} Elucidating the intermolecular structure in a complex liquid such as 1-*n*-butyl-3-methylimidazolium hexafluorophosphate ([bmim][PF₆]) is a challenging task that

* Author to whom correspondence should be addressed. E-mail: bala@jncasr.ac.in.

[†] E-mail: bhargava@jncasr.ac.in.

demands the combined use of experimental, computational, and theoretical probes. In this effort, scattering experiments are handicapped by the lack of phase information. It is also quite difficult to obtain partial pair correlation functions of such systems directly from experiments. Although atomistic computer simulation methods such as molecular dynamics (MD) or Monte Carlo that employ empirical potentials have redressed this lack of knowledge to a large extent, doubts on the transferability of the potential parameters across various condensed systems limit their capability to truthfully represent ILs.

Given this background and the importance of the systems involved, it is crucial that a reliable microscopic picture of the intermolecular structure of the mixture is obtained. Ab initio molecular dynamics simulations based on density functional theory have had considerable success in the recent past in the elucidation of the structure and dynamics in a variety of complex systems, including ionic liquids.^{48–54} In this work, we report results of such a study on the CO₂–[bmim][PF₆] mixture in the hope that it will augment the current knowledge. As a reference system, we present results of Car–Parrinello MD simulations on pure [bmim][PF₆] as well. Our methods are detailed in the next section, followed by a presentation of the results. We end with conclusions drawn from our study.

2. Methodology and Simulation Details

A mixture of CO₂ and a room-temperature ionic liquid, 1-*n*-butyl-3-methylimidazolium hexafluorophosphate was studied using ab initio molecular dynamics simulations. The simulated system consisted of 12 units each of [bmim] and [PF₆] ions and 28 CO₂ molecules, amounting to 70 mol % of CO₂ in the mixture. The simulations were carried out at 298 K at extrapolated experimental density^{41,43,55,56} using the CPMD^{57,58} code. This system with a total of 468 atoms was simulated in a cubic box of edge length 17.56 Å. The initial configuration for the CPMD run was generated by equilibrating the system at room temperature and experimental density for a duration of 8 ns using classical MD with a force field as mentioned later. Norm-conserving pseudopotentials of the Troullier–Martins form⁵⁹ were employed to take into account the effect of the core electrons and the nuclei. Gradient-corrected exchange and correlation functionals prescribed by Becke⁶⁰ and Lee, Yang, and Parr⁶¹ were employed. The initial configuration for the CPMD run was obtained from a classical MD simulation of 8 ns in duration. A plane wave basis set with an energy cutoff of 90 Ry was used to expand the electronic orbitals. This value of the cutoff was chosen after checking for the convergence of the forces on ions as a function of increasing energy cutoff. Three-dimensional periodic boundary conditions were applied to obtain bulk behavior. All of the hydrogens in the system were substituted by deuterium to enable the use of a larger time step of integration. Prior to the CPMD run, the electronic degrees of freedom were quenched to the Born–Oppenheimer surface. During the CPMD simulations, a fictitious electron mass of 700 a.u. was employed. The kinetic energy of the ions was controlled using the Nosé–Hoover chain thermostat.⁶² The equations of motion were integrated with a time step of 5 a.u. (around 0.12 fs) over a length of 13.9 ps out of which the last 10.4 ps of data were used for analysis. The conservation in total energy was 8 parts in 10⁹ over a duration of 7 ps.

To study the differences in the structure and dynamics upon addition of CO₂ to [bmim][PF₆], an additional CPMD simulation of pure [bmim][PF₆] containing 12 ion pairs was carried out at room temperature and at a density of 1.36 g/cm³. This system consisted of a total of 384 atoms within a cubic box of edge

length 16.09 Å. The CPMD trajectory length was 11 ps, out of which the last segment of 7.9 ps in duration was used for analysis. Other details of the run are the same as that for the mixture.

In addition to these CPMD calculations, classical molecular dynamics simulations (using empirical potentials) were carried out on a mixture containing 70 mol % of CO₂. This system consisted of 324 ion pairs of [bmim][PF₆] and 756 CO₂ molecules, together accounting for a total number of 12 636 atoms. The model was fully flexible with respect to the [bmim]–[PF₆] ion pairs, while the bond lengths of the CO₂ molecules were constrained in accordance to the EPM2 interaction potential.⁶³ The simulations were carried out in a cubic box of edge length 53.0 Å with periodic boundary conditions consistent with the cubic symmetry. Nosé–Hoover chain thermostats⁶² were used to maintain the temperature of the system at 298 K. The form of the interaction potential and parameters for the [bmim][PF₆] ion pair were adopted from the work of Lopes et al.,⁶⁴ which is consistent with OPLS/AA and AMBER schemes. The PF₆ ion was made fully flexible by adding the stretching and bending potentials derived from earlier work.⁶⁵ The interaction potential parameters for the CO₂ molecules were obtained from the work of Harris and Yung.⁶³ Cross-interactions were treated using Lorentz–Berthelot rules. On the basis of the procedures outlined here, we have recently studied the liquid–vapor interface of [bmim][PF₆].⁶⁶ Coulombic interactions were handled using the Ewald summation method. Exactly 10 239 reciprocal lattice space vectors were used to calculate the Coulomb energy. Nonbonded interactions were calculated up to a distance cutoff of 13 Å. The equations of motion were integrated using the multiple time step algorithm, RESPA,⁶⁷ in which nonbonded interactions beyond 6 Å and within 13 Å were calculated with a time step of 3 fs, and those within 6 Å were calculated with a time step of 1.5 fs. The torsional forces were computed every 0.75 fs, and the bending and stretching degrees of freedom were integrated with a fine time step of 0.375 fs. The positions of the atoms in the system that were used for analysis were stored every 0.9 ps.

A bin width of 0.2 Å is used in the calculation of radial distribution functions (RDFs), except for the crystalline RDFs for which a finer bin width of 0.001 Å is used.

For the calculation of molecular dipole moments, 34 instantaneous configurations each of the pure [bmim][PF₆] system and of the mixture were selected, and the centers of maximally localized Wannier orbitals^{68–72} were obtained using the CPMD code. The dipole moments of molecules or ions were calculated by assigning a charge of $-2e$ for the Wannier centers and atomic valence charges for the ion centers. The dipole moment for a charged system depends on the choice of the origin of the coordinate system. Here, we follow the earlier work of Lynden-Bell and co-workers⁷³ on a similar calculation performed for liquid 1,3-dimethylimidazolium chloride. The dipole moment in the classical system was calculated using the partial charges on the atoms.

3. Results and Discussions

A schematic of [bmim][PF₆] along with the atom numbering scheme and the coordinate system employed for the calculation of dipole moments is presented in Figure 1 to aid further discussion.

A few of the bond lengths and bond angles obtained from the geometry-optimized structure of the cation or anion in the gas phase (i.e., under isolated conditions) are compared against the values in the crystal⁷⁴ in Table 1. The geometry of the

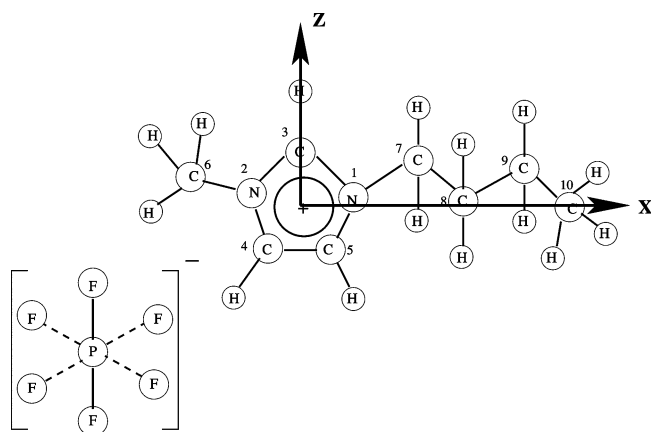


Figure 1. Schematic representation of [bmim][PF₆] along with the atom numbering scheme. The axes define the coordinate system employed in the calculation of the dipole moment of the cation. The y-axis is perpendicular to the plane of the imidazolium ring.

TABLE 1: Comparison between the Geometry of [bmim][PF₆] Determined from the X-ray Crystal Structure⁷⁴ and That from a CPMD-Optimized Configuration in the Gas Phase (Isolated Conditions)

type	experiment	CPMD
bond length (Å)		
N1-C3	1.33	1.35
N1-C5	1.38	1.39
N2-C3	1.32	1.34
N2-C6	1.47	1.48
N1-C7	1.47	1.50
C4-C5	1.35	1.37
C9-C10	1.52	1.54
P-F	1.60	1.71
angle (deg)		
N1-C3-N2	108.8	108.9
N1-C4-C5	107.2	107.3
C3-N1-C7	125.6	125.6
C3-N2-C6	125.3	125.7

imidazolium ion is in good agreement with the crystal structure. Most bond lengths of the cation are reproduced within 1.5% of experiment. The planarity of the ring too is reproduced in the ab initio calculations. However, the calculated P-F distance is farther from that in the crystal by 6%. This appears to be a limitation of density functional theory.⁷⁵ We wish to note here that the fluorine pseudopotential itself was tested by optimizing the geometry of an isolated F₂ molecule. In F₂, the F-F distance was found to be 1.435 Å, which is to be compared against a value of 1.4119 Å in experiments.⁷⁶

Ab initio MD simulations of liquids demand large computational resources although the accessible time and length scales are rather limited. Under these circumstances, one needs to ensure that the durations of the trajectory allotted for equilibration and analyses are adequate. In addition, since ILs in general and [bmim][PF₆] in particular are viscous (with viscosity of around 200 cP at 300 K), it is conceivable that the properties obtained from such limited CPMD simulations could reflect that of the initial configurations. However, we have found several crucial structural quantities to differ between the classical MD and the AIMD simulations. Hence, the results reported here are less likely to be influenced by any bias in the initial configuration.

In the subsections that follow, we present results on the arrangement of CO₂ molecules in the IL. It is thus natural to ask whether the CO₂ molecules sample the configuration space well. This can be answered by studying the magnitude of their displacements. The values of mean-squared displacements of

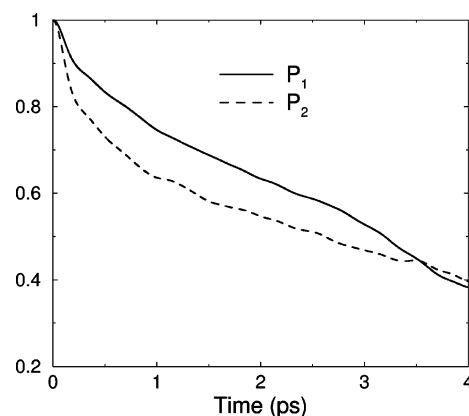


Figure 2. First- (P_1) and second-order (P_2) Legendre-polynomial-based rotational time correlation functions of the backbone vector of CO₂ molecules, as obtained from CPMD simulations of the [bmim][PF₆]-CO₂ mixture.

TABLE 2: Maximum and Mean-Squared Displacements of CO₂ Molecules and the Ions over 8 ps

ion/molecule	maximum displacement (Å)	mean-squared displacement (Å ²)
CO ₂	5.6	4.7
[PF ₆]	3.0	2.4
[bmim]	3.0	2.8

various species in the system, including that of CO₂, are provided in Table 2. Over a duration of 8 ps, the mean-squared displacement of CO₂ has been calculated to be 4.7 Å² with a maximum displacement of 5.6 Å. For the sake of completeness, the values obtained for the anion and the cation are also presented in Table 2.

Another quantity of interest that demonstrates the mobility of CO₂ molecules is the reorientational time correlation function of the CO₂ backbone that is shown in Figure 2. The P_1 and P_2 functions (first- and second-order Legendre polynomials) decay to values of around 0.4 in 4 ps, indicating that, on average, every CO₂ molecule would have explored the local orientational landscape within the time scales for which we have simulated the mixture.

3.1. Radial Distribution Functions. The partial radial distribution functions of the ions calculated from the CPMD, classical MD runs, and the crystal for pure [bmim][PF₆] are presented in Figures 3a and 3b. Here, the anion is represented by the phosphorus atom, and the cation by the center of the imidazolium ring. The anion-anion radial distribution function obtained from CPMD exhibits significant differences with that from the classical MD simulation. The RDF for PF₆-PF₆ seems to show a shoulder at around 6 Å that is absent in the classical MD data. Significantly, the anions approach each other closer in the CPMD trajectory. This may be attributed to the natural inclusion of electronic polarization of the anions in CPMD that is missing in the classical interaction potential.⁷⁷ A slight increase in the intensity and a hump near 4.7 Å are observed in the [bmim]-[PF₆] RDF obtained from CPMD. Interestingly, the first peak in the crystalline RDF is also present at this distance. Relatively minor differences in the cation-cation $g(r)$ between classical and CPMD data are ignored in the present discussion due to paucity of statistics. Comparison of CPMD data with that of crystal RDFs reveals strong similarities between the intermolecular structure in the liquid and that in the crystal.

Several MD simulation studies on the IL [bmim][PF₆] using empirical potentials have been reported.⁷⁸⁻⁸¹ The partial radial distribution functions reported in these studies have been found

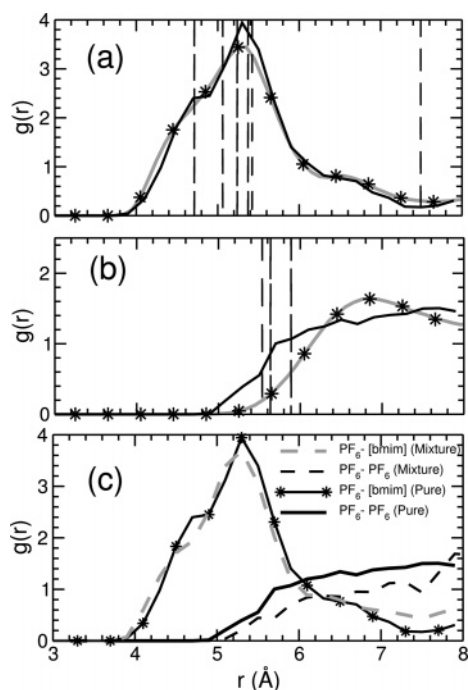


Figure 3. Comparison of RDFs obtained from classical MD and CPMD simulations in pure [bmim][PF₆] as well as in the [bmim][PF₆] crystal.⁷⁴ (a) [bmim]–[PF₆]; (b) PF₆–PF₆. The solid black line represents the CPMD data, the solid gray line with stars represents the classical MD results, and the dashed black line corresponds to the crystal. (c) Comparison of RDFs obtained from the CPMD data in the presence and absence of CO₂. Symbols are shown infrequently for clarity.

to be different from one another and to varying extents with our ab initio results.³⁹ The potential model used by Morrow and Maginn⁷⁹ and Margulis et al.⁷⁸ predicts a higher peak intensity for the C3–P RDF compared to our ab initio results (data not shown).

The effect of CO₂ on the structure of IL in the mixture can be seen from Figure 3c, which compares various partial RDFs obtained from CPMD simulations in the presence and in the absence of CO₂. In tune with earlier reports,^{38,40} there is no noticeable difference in the partial RDFs. However, the anion–anion RDF seems to be strongly influenced by the presence of CO₂. The corresponding coordination number at 8 Å is 3.2 in the mixture compared to a value of 5.4 in the pure liquid. This decrease is likely due to the stronger anion–CO₂ interaction, which is discussed in detail in the following sections. The existence of solvent (CO₂) separated ion pairs can be discerned from the marginal reduction in the intensity of the cation–anion RDF. The similarity between the RDFs of the mixture and of the pure IL can be rationalized. Physical measurements⁵⁵ and earlier simulations⁴⁰ have shown that the addition of CO₂ does not change the molar volume of the ionic liquid significantly. In particular, Berne and co-workers⁴⁰ have demonstrated that the CO₂ molecules prefer to occupy the void regions present in the IL.

Figure 4a compares the radial distribution functions, obtained from CPMD simulations, for fluorines of the anion around the ring hydrogen H(C3) in the mixture and in the pure liquid. The fluorine atoms are found to be nearer to the ring hydrogen H(C3), and the first peak height is more intense in the mixture by about 11% over its value in the pure system. A part of this change could also have arisen from the minor differences in the molar volumes of the two systems studied.

Crucial differences are noticed in the RDFs of the fluorine atoms of the anion and the ring hydrogen H(C3) between the

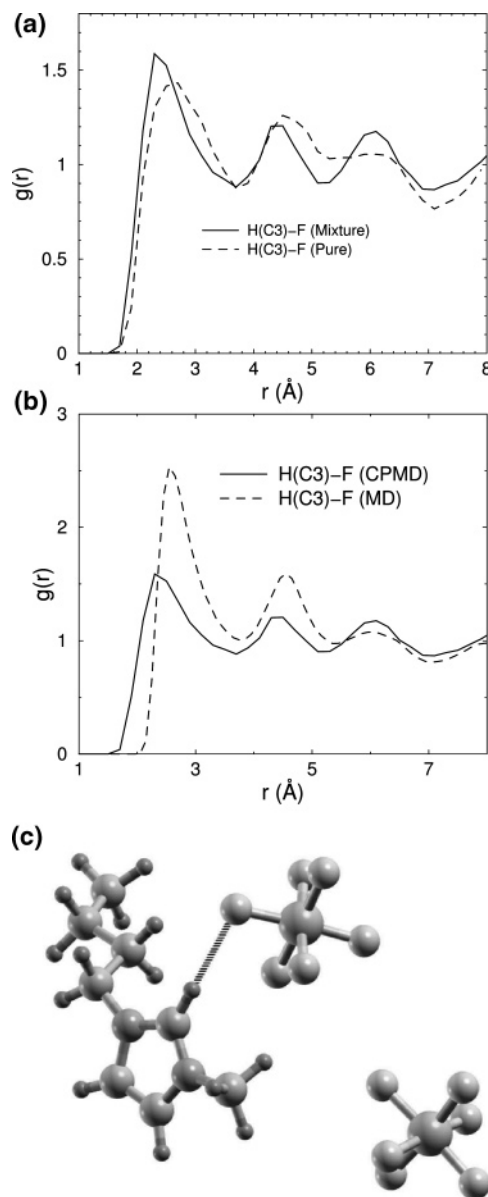


Figure 4. (a) Comparison of RDFs between ring hydrogen H(C3) and fluorine, as obtained from CPMD simulations in the presence and absence of CO₂. (b) Comparison of RDFs between ring hydrogen (H(C3)) and fluorine in the mixture, as obtained from CPMD and from classical MD simulations. (c) Snapshot of part of the pure [bmim][PF₆] system from the CPMD trajectory, showing the hydrogen bond between H(C3) and fluorine of the anion.

CPMD and classical MD simulations of the mixture, as shown in Figure 4b. In the former, a clear shift toward smaller distances is observed in the position of the first peak. Further, a reduction in the peak height is also observed. It can thus be safely said that the ring proton H(C3) forms a hydrogen bond with the fluorine atoms of the anion. Some of the classical models⁸⁰ are found to overestimate the hydrogen bonding between the ring proton H(C3) and fluorines of the anion. In view of the distances involved, this hydrogen bond would be characterized as “weak”.⁸² On the basis of a maximum H–F distance of 2.5 Å and a minimum value for the C–H–F angle of 160° to define a hydrogen bond, the fraction of cations in pure [bmim][PF₆] that forms such hydrogen bonds is estimated to be around 8%. This is to be compared against a value of 3.7% obtained from classical MD simulations. A snapshot of a part of the bulk system selected from the CPMD trajectory is shown in Figure 4c⁸³ as an example of the cation–anion hydrogen bond.

Although empirical potential MD predicts nearly the same percentage of cation-anion hydrogen bonding in the mixture compared to that in the pure system, CPMD results show a marginal increase in the percentage of hydrogen bonding, which is around 11.5% in the mixture. The [bmim][PF₆] crystal is reported to contain 7 hydrogen bonds per cation,⁷⁴ based upon liberal hydrogen bond criteria that the H-F bond length be less than 2.7 Å and the C-H-F angle be greater than 90°. Using these criteria, it was found that there are, on an average, 10 hydrogen bonds per cation in the neat liquid simulated using CPMD. To summarize, although the density functional theory (DFT)-based simulations predict a higher propensity for hydrogen bonds in the ionic liquid compared to classical simulations, their fraction and strength appear to be weak. This is particularly valid for an anion that is weakly basic such as the hexafluorophosphate studied here. The tetrafluoroborate anion could form a stronger cation-anion hydrogen bond. Formation of strong cation-anion hydrogen bonds has been reported earlier in another IL, 1,3-dimethylimidazolium chloride ([dmim]-[Cl]),^{48-50,84,85} We also observe a rather small, but non-negligible, increase in the number of hydrogen bonds in the liquid upon addition of CO₂. This needs further examination.

The radial distribution of CO₂ molecules around the ions and CO₂ is shown in Figure 5a. The narrower first peak in the case of the anion shows that the CO₂ molecules are more ordered around the anion than around the cation. CO₂ molecules are also proximal to the anion center rather than to the ring center of the cation. The first peak of the anion-CO₂ $g(r)$ is at 4.3 Å with a coordination number of 4.6 up to the first minimum at 5.9 Å, whereas the cation-CO₂ $g(r)$ peaks at 5.3 Å with a coordination number of 8.7 up to the first minimum at 7.3 Å. The difference in the mean P-F bond distance between theory (1.7 Å) and experiment (1.6 Å) may have a minor effect on the RDF between PF₆ and CO₂. In reality, the pair correlation function may be shifted by about 0.1 Å with a marginal reduction in the P-C coordination number.

The coordination number of CO₂ around the anion, which is 4.6, compares with the value of 4.0 estimated from X-ray scattering experiments.⁴¹ The reported⁴¹ interatomic distance between phosphorus and the carbon atom of CO₂ (P-C) is 3.59 Å, which is quite small when compared to the observed first peak position in our CPMD simulations and also earlier empirical potential MD simulations. Also, the interatomic distance of 3.59 Å for P-C demands that the distance between the atoms of the anion and those of CO₂ to be less than the sum of their van der Waals radii. It is thus likely that the peak at 3.6 Å observed in the total $g(r)$ in scattering experiments is likely to come from CO₂-CO₂ pairs rather than from CO₂-PF₆ pairs.

However, our simulations also found that each CO₂ interacts with two PF₆ ions, in agreement with the experiments.⁴¹ As discussed earlier, this strong coordination of CO₂ around the anion influences the anion-anion RDF in the mixture, which differs from that in the pure system. The CO₂-CO₂ $g(r)$ peaks at 3.7 Å with a coordination number of 4.3 up to the first minimum at 5.9 Å. From the amplitude of the peaks in Figure 5a, it is evident that the CO₂ molecules are preferentially found near the anion. Another novel finding of the current work is the characterization of the intermolecular structure between CO₂ and the cation. We have observed that among the ring hydrogens the one attached to C3 is closest to the oxygen atom of CO₂. It exhibits a clearer coordination shell when compared to those of the other two ring hydrogens. Figure 5b compares the RDF of the oxygen atoms of CO₂ around the ring hydrogen H(C3),

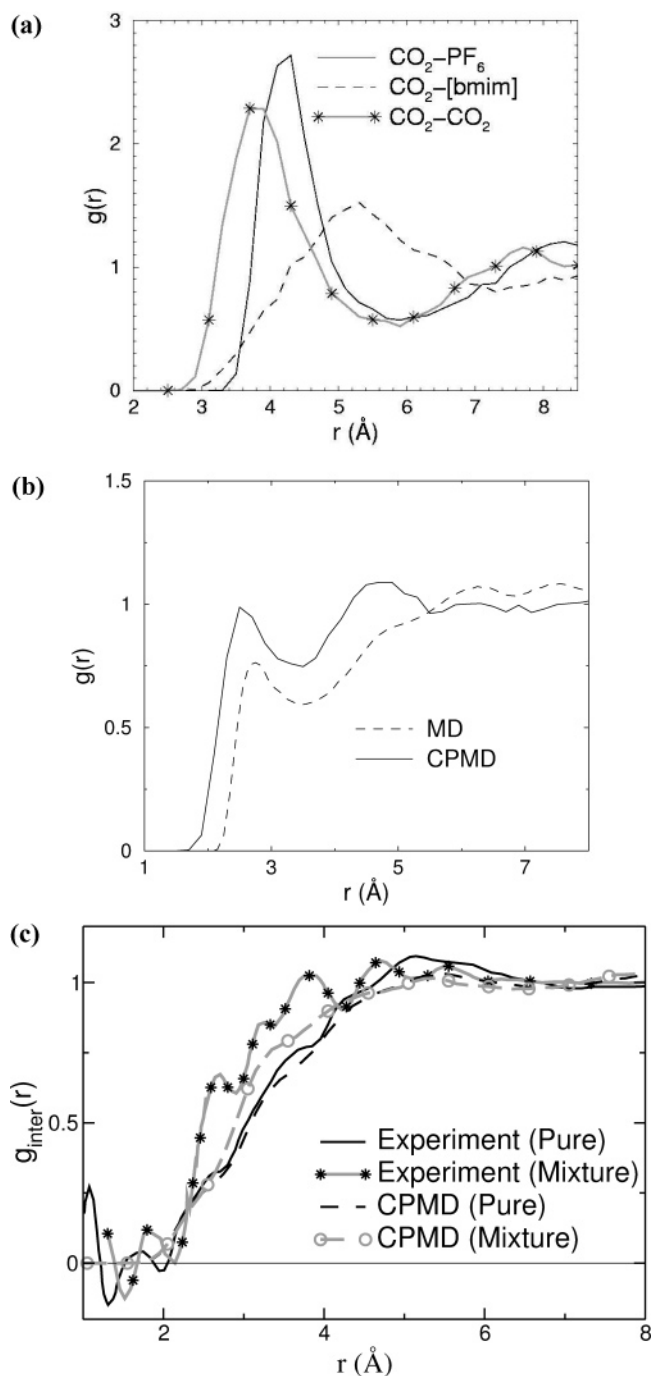


Figure 5. (a) Partial RDF of CO₂ around the cation, the anion and CO₂ in the mixture, as obtained from CPMD simulations. The position of the carbon atom is taken to represent the CO₂ molecule. The cation is represented by the geometric center of the imidazolium ring while the phosphorus atom denotes the anion location. (b) Comparison of the RDF of oxygen atoms of CO₂ around the ring hydrogen H(C3) in the mixture, as obtained from CPMD and classical MD simulations. (c) Comparison of the intermolecular RDFs obtained from CPMD simulations with experiments⁴¹ for pure [bmim][PF₆] and the [bmim][PF₆]-CO₂ mixture. The symbols are shown infrequently for clarity.

as obtained from classical and CPMD simulations. The increased interaction of the oxygens with H(C3) suggests the formation of a weak hydrogen bond in the CPMD simulations. Using the liberal criteria for hydrogen bonding, i.e., H-O distance less than 2.7 Å and C-H-O angle greater than 90°, it was found that the oxygen atom of CO₂ was hydrogen-bonded to the ring hydrogen H(C3) for about 5% of the time in CPMD versus 2% in the classical MD simulations. The absence of such an

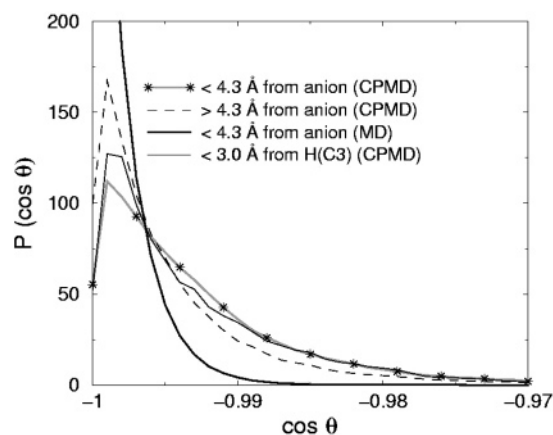


Figure 6. Intramolecular O–C–O angle distributions in the CO₂ molecule. The distances in the legend are those between the carbon atom of CO₂ and the phosphorus atom of the anion (or the H(C3) atom of the cation). Symbols are shown infrequently for clarity.

interaction in the classical potential model is striking and needs to be redressed.

In Figure 5c, we compare the intermolecular RDFs obtained from our simulations with the X-ray scattering results of Kanakubo et al.⁴¹ A good agreement between simulation and experiment is observed for pure [bmim][PF₆] while the prominent oscillations found in the experimental data for the [bmim]–[PF₆]–CO₂ mixture are not seen in the simulation. The reasons for this absence are unclear and need to be investigated further. They could point to system size effects, limitations in DFT, or numerical issues in obtaining the function from the scattering data in experiments. Note that the peaks are observed at the corresponding positions in the partial pair correlation functions obtained from simulations; however they are washed out during averaging to obtain the intermolecular RDF. Specifically, we can attribute the feature in the experimental data present at 3.1 Å to intermolecular oxygen–oxygen distances between CO₂ molecules. It should be noticed that the trend seen in the experimental RDF between the pure system and the mixture is qualitatively reproduced in the simulation. The magnitude of increase in the intensity of the RDF upon adding CO₂ is smaller, and the oscillations are absent in the simulation.

3.2. Intramolecular Angle Distribution of CO₂. Having obtained an understanding of the intermolecular structure of [bmim][PF₆] and the nearest neighbor environment around CO₂ in this IL, we turn our attention to its effect on the intramolecular structure of CO₂ molecules. As discussed in the Introduction, a polar neighborhood can force CO₂ molecules to adopt instantaneous nonlinear geometries. Shown in Figure 6 are the probability distributions of the O–C–O angles of CO₂ molecules under various conditions. The classical MD data employing a harmonic bending potential predict a distribution that is closest to a linear geometry. The CPMD data exhibit more propensity for instantaneous deviations from linearity. A striking feature is the difference between the angle distributions obtained from the CPMD simulation when the CO₂ molecule is closer to and farther from the PF₆ anion. The former are more bent than the latter. We choose the position of the first peak of the C–P *g*(*r*), i.e., 4.3 Å, as a distance cutoff to distinguish between the two sets of CO₂ molecules. The figure illustrates this aspect for CO₂ molecules within 4.3 Å from the phosphorus atom of an anion as well as for those CO₂ molecules that are at least more than 4.3 Å away from every anion. Further, we observe that the extent of bending of CO₂ molecules that are within 3 Å from the acidic hydrogen (H(C3)) of the cations is similar to

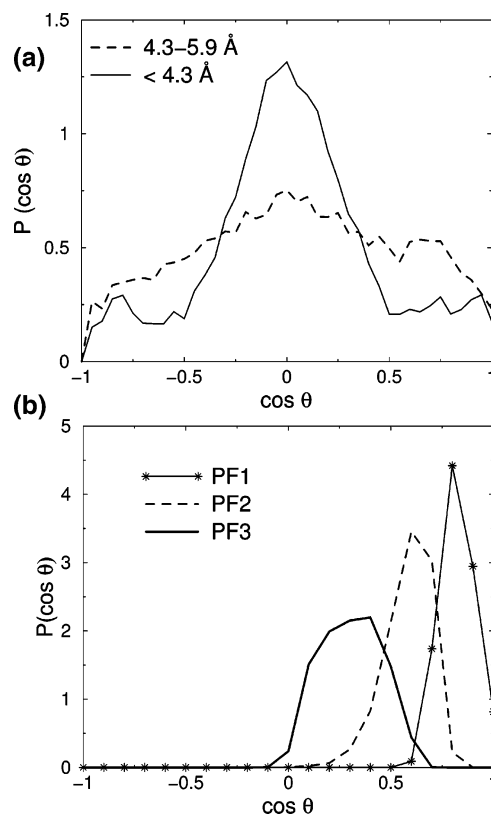


Figure 7. (a) Orientation of the CO₂ molecules around the PF₆ anion in the mixture. θ is the angle between the backbone vector of CO₂ and the vector connecting the phosphorus atom of the anion to the carbon atom of CO₂ molecule in the range of distances mentioned in the legend. The data are obtained from CPMD calculations. (b) Distribution showing the preferred location of the CO₂ molecule around the anion, as obtained from CPMD simulations. θ is the angle between the vector joining the carbon atom of CO₂ with the phosphorus atoms of the anions that are within 4.3 Å and the vector along the P–F bond. F1, F2, and F3 corresponds to the first, second and third nearest fluorine to the carbon, respectively.

those which are present closer to the anions. It thus appears that the cation too is sufficiently capable of polarizing the electronic and geometric structure of CO₂ for it to adopt nonlinear geometries.

3.3. Orientations of CO₂ Molecules. **3.3.1. Orientation around Anions.** The orientational preference exhibited by a CO₂ molecule in the first coordination shell around the PF₆ anion in the [bmim][PF₆]–CO₂ solution has not been conclusive from the literature reports. Earlier MD simulation studies have concluded that the CO₂ molecule is aligned tangential to the spherical PF₆ anion.^{38,40} However, recent X-ray scattering experiments⁴¹ argue that the CO₂ molecules penetrate the hollow voids in the PF₆ sphere. The ab initio MD results reported here agree with earlier simulations that were carried out using empirical potentials.

Plotted in Figure 7a are the probability distributions for the angle between the vectors connecting the two oxygen atoms of a CO₂ molecule and the vector that connects the phosphorus atom of PF₆ to the carbon atom of CO₂. The probability of the CO₂ molecules to be located tangential to the anion is larger when they are closer to the anion. However, this orientational preference decreases with an increase in the distance between CO₂ and the anion. Shown in the figure are two distributions, one for CO₂ molecules that are within 4.3 Å of the anion center and the other for CO₂ molecules that are present between 4.3 and 5.9 Å. The behavior of the function in classical MD is similar to that in CPMD. Given the fact that most CO₂ molecules

would have undergone one or more complete rotations within the time scales of the CPMD run, it would be safe to conclude that the DFT-based simulations reported here agree quite well with earlier classical simulations.^{38,40}

3.3.2. Orientation of CO₂ with Reference to Fluorine Atoms of Anions. To determine the most favorable locations of the CO₂ molecules around the anions, we design a geometric analysis as follows. The three nearest fluorines of an anion that are present within 4.3 Å (which is the position of the first peak position in the anion-CO₂ $g(r)$) of a CO₂ molecule were determined. Subsequently, the distributions of the angle between the C-P vector (where C is the carbon atom of the CO₂ molecule) and the three P-F vectors were determined. These are presented in Figure 7b. The MD results are identical to the CPMD data. All three distributions fall entirely in the positive domain of $\cos(\theta)$, proving that the carbon atom of the CO₂ is present in the same octant defined by the three vectors. The most probable values of the angles are found to be 37°, 53°, and 66°, respectively. These values indicate that the carbon atom of the CO₂ molecule is likely to be present in the octahedral void of the anion formed by these three fluorine atoms. In view of the rather broad nature of the distribution related to the PF₃ vector (the third nearest fluorine to the CO₂), we wish to caution the reader that this result should be construed only as indicative of a preference for the carbon atom to be present in the octahedral hole. Not every carbon atom can be expected to occupy this site in a precise manner. In essence, such distributions are the *raison d'être* to perform computer simulations of the liquid state, as compared to quantum chemical calculations of isolated molecules or ion pairs. To summarize, we observe a strong preference for the carbon atom of CO₂ to be present in or around the octahedral voids of the anion.

There are eight such voids in the anion. As discussed earlier, at this mole fraction of CO₂, the anion is surrounded by about 4.6 CO₂ molecules within a distance of 6 Å. This gives an effective percentage of occupation of the octahedral voids as 58%. Beyond this magnitude, CO₂-CO₂ repulsion could be expected to dominate over the interaction strength with the anion. Note that the maximum solubility of CO₂ in [bmim][PF₆] is slightly more than 70 mol %.^{31,43} We speculate that the underlying reason for this value of maximum solubility could be due to the fact that one has exhausted the maximum number of favorable sites near the anion that could be occupied. Further simulation studies (even classical MD simulations with refined potentials would do) as a function of CO₂ concentration could validate this conjecture.

3.4. Density Maps. 3.4.1. SDFs of Anions around Cations.

The spatial distribution functions (SDFs) of the anions around the cation in the case of pure [bmim][PF₆] obtained from classical MD and CPMD trajectories are presented in Figure 8. They show the probability density distribution of the anion (phosphorus) around the cation at an isosurface value of 0.0375 atoms/Å³, which is 13 times higher than the average density of the anions in the liquid. In the figure, parts a and b represent classical MD data whereas parts c and d are from CPMD. In Figures 8a and 8c, the ring plane of the cation is tilted to the plane of the paper around the C3-H vector. The classical MD data shows two clear lobes of density around H(C3), above and below the ring plane, which is also evident from Figure 8b. Note that there is negligible presence of the anion exactly above the acidic proton. A considerable density of anions is also observed near the ring hydrogens H(C4) and H(C5). In contrast, the CPMD data shows a finite probability for the anions to be

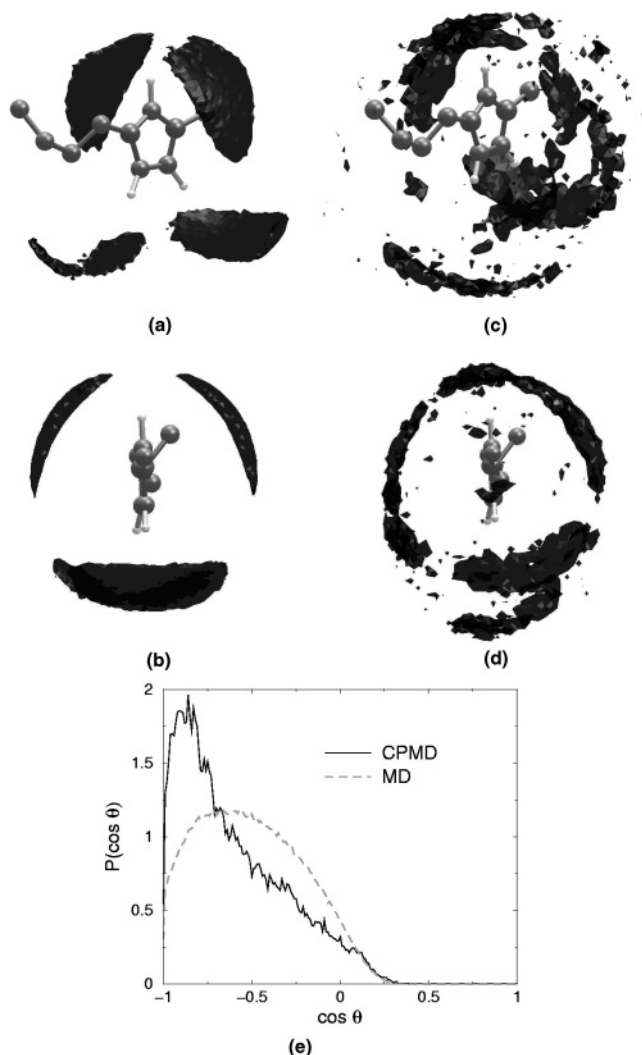


Figure 8. Spatial density distributions of the anions around the cation in pure [bmim][PF₆], as obtained from classical MD and CPMD data at an isosurface value of 0.0375 atoms/Å³: (a) tilted view, classical MD; (b) side view, classical MD; (c) tilted view, CPMD; (d) side view, CPMD. The hydrogen atoms in the methyl and butyl groups are not shown for clarity. (e) Distribution of the angle between the vectors connecting H(C3)-C3 and H(C3)-P when the phosphorus atom is within 4.0 Å from H(C3), as obtained from classical MD and CPMD simulations.

present above H(C3), which was also observed in our earlier work on [mmim][Cl].⁵⁰

The angular distribution of anions around the cation and the specific differences between the classical MD and CPMD data have been highlighted through the above analyses. We quantify this observation by studying the angle of approach of the anion as it forms a hydrogen bond with the H(C3) of the cation. Shown in Figure 8e is the distribution of the angle between the vectors formed by C3-H(C3) and H(C3)-P whenever an anion is within 4.0 Å from H(C3). Significant differences are observed between the results of classical and CPMD simulations. While the latter shows a strong preference for the anion to approach the acidic hydrogen along its C-H bond vector, classical MD predicts a rather weaker orientational preference.

Within our statistical accuracy, no differences were observed in the SDFs obtained for the pure [bmim][PF₆] and mixture from the CPMD data (not shown).

3.4.2. SDFs of CO₂ around Anions. The SDFs of the carbon and oxygen atoms of CO₂ molecules that are located around an anion are presented in Figures 9a and 9b. Black represents the

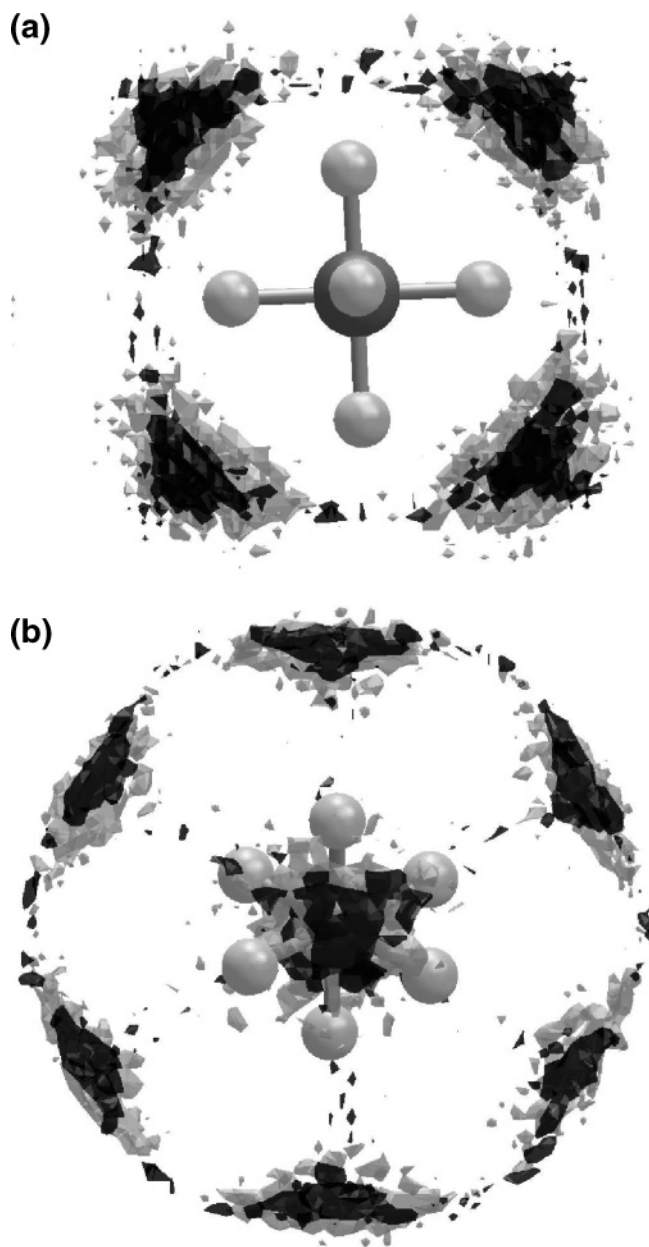


Figure 9. (a) Spatial density distribution of the CO₂ molecules around the anion in the mixture at an isosurface density of 0.02125 atoms/Å³ for carbon (gray) and 0.0425 atoms/Å³ for oxygen (black). The data are obtained from classical MD simulations. (b) Same as Figure 9a, but in a different orientation.

oxygen density, and gray the carbon density, as obtained from classical MD simulations. The CPMD data are not shown due to a paucity of statistics. Both carbon and oxygen densities are highest in the octahedral voids around the anions. Recall that the coordination number of CO₂ around the anion is 4.6, which suggests that not all of the eight octahedral voids are occupied by CO₂ in every case, but only around half of them will be occupied by the CO₂ around each anion. However, eight distinct lobes are seen in Figure 9b, as the data are averaged over the anions and over the MD trajectory. Figure 9a shows the density of CO₂ around the anion in an orientation such that one of the P–F bond directions is perpendicular to the plane of the paper, and in Figure 9b, the same data are shown as seen from the top of an octahedral void. This distribution is favored as the carbon can interact with three of the fluorines via possibly an electron donor–acceptor interaction. At a given octahedral void location, the densities of both the carbon and the oxygen atoms overlap

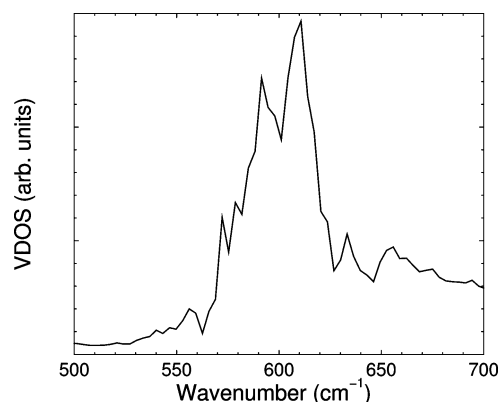


Figure 10. Vibrational density of states of CO₂ molecules in the CO₂ bending mode region.

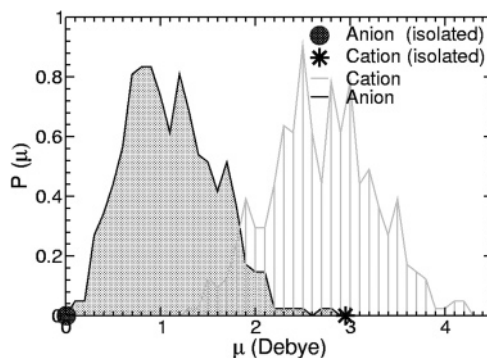


Figure 11. Distributions of instantaneous dipole moments of the cation and the anion in the pure [bmim][PF₆] system along with the values for the structure-optimized cation and anion under isolated conditions.

as their distance from the central phosphorus atom is the same. This observation too supports the model of a tangential orientation of the CO₂ molecule around the spherical anion.

3.5. Vibrational Dynamics. The vibrational density of states obtained from the Fourier transform of velocity autocorrelation function for the atoms of CO₂ is shown in Figure 10. The split in the bending mode of CO₂ is clearly seen, which is qualitatively consistent with the experiments of Kazarian and co-workers.³⁶ Density functional theory calculations are known to predict lower vibrational frequencies relative to experiment.⁸⁶ This has specifically been observed for supercritical CO₂ as well earlier.⁸⁷ The splitting of the OCO bending mode can be rationalized as due to the interaction of the CO₂ molecules with the ions of [bmim][PF₆].

3.6. Dipole Moments. The instantaneous total dipole moment distributions of the anions and cations calculated from the Wannier centers obtained from CPMD code are presented in Figure 11. The coordinate axes chosen for the calculation are shown in Figure 1. The dipole moment for an ion is dependent on the choice of the coordinate system. Hence, the values reported here need to be interpreted not for their absolute magnitudes but for the trends that they exhibit. The geometric center of the imidazolium ring was chosen as its origin. The *z*-axis was along the line joining the center of the ring to C3, the *y*-axis was perpendicular to the ring plane, and the *x*-axis was perpendicular to the *y*- and *z*-axes. The spherical PF₆ ion carries zero dipole moment under isolated conditions, as expected. However, thermal fluctuations in its geometry as well as its capacity to be polarized in the ionic liquid environment lead to nonzero values of dipole moment for instantaneous configurations. The initial configuration for the geometry optimization procedure of the isolated cation (gas phase) was

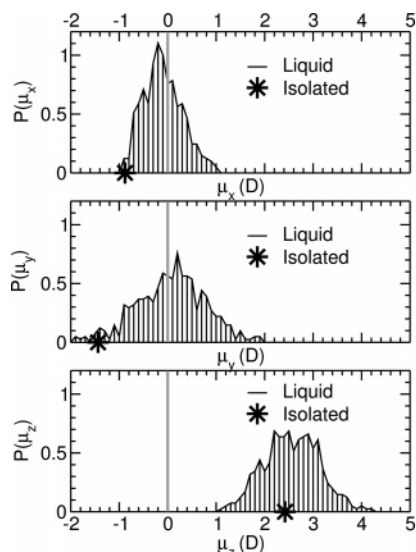


Figure 12. Distribution of components of the instantaneous dipole moments of the cation in the pure [bmim][PF₆] system along with the values for the structure-optimized cation under isolated conditions.

taken from the crystal structure.⁷⁴ Presented in Figure 12 are the distributions of the components of instantaneous dipole moments of the cations in pure [bmim][PF₆] obtained from CPMD simulations along with the corresponding value of the isolated cation mentioned above. The broad nature of the distribution of the *x*- and *y*-components is due to the many possible conformations of the butyl chain. The width in the *z*-component is due to these conformations as well as to the polarization of the C–H(C3) bond.

Shown in Table 3 are the instantaneous total dipole moments and their components of anions and cations obtained from classical MD and CPMD data. The total dipole moment of the anion obtained from the classical MD data is 0.31 ± 0.13 debye, which is very small compared to the CPMD value of 1.06 ± 0.48 debye. The dipole moment in the classical MD model with time-independent charges arises only due to geometric fluctuations. However, in CPMD, it arises from such fluctuations as well as due to changes in the electron distribution near the ions. The distributions of dipole moments obtained from CPMD calculations can guide the development of polarizable interaction models.⁸⁸ The cation is also found to possess a higher dipole moment compared to the classical values. Similar results were reported recently for another ionic liquid, [mmim][Cl], which was found to be more polarized in the liquid phase when compared to the gaseous environment.⁷³ It was also noticed that relative to pure [bmim][PF₆] the cations in the mixtures were marginally less polarized (data not shown). This can be rationalized as due to the presence of the charge neutral species CO₂ in the mixture, which reduces the Coulombic forces felt by the cations.

4. Conclusions

Initial attempts made over the past few years to study the molecular organization in room-temperature ionic liquids using ab initio MD simulations have been successful.^{48–50} These calculations were performed on [mmim][Cl], which melts only at 395 K and is thus not so appealing to physical and synthetic chemists interested in room-temperature properties. The work reported here has been carried out on an IL that is relevant to experimentalists⁸⁹ and further extends the existing knowledge on the microscopic details of these systems. In the absence of experimental data on the intermolecular structure of the pure IL and its solution with CO₂, the results of ab initio MD simulations will also be of great help for computational studies based on classical force field models. The structural data reported here can form a baseline for the refinement of empirical potentials⁹⁰ and can serve as an essential building block to construct hierarchical models that aid in studying larger length and time scales.

Results from the AIMD study of [bmim][PF₆] and its mixture with CO₂ show some significant differences with that from classical MD simulations. Although classical potential parameters predict the distribution of the ions around each other and that of CO₂ around the cation and anion to a good accuracy, they differ from the AIMD data in some respects. AIMD predicts the formation of a weak hydrogen bond between H(C3) of the cation and fluorine atoms of the anion, a feature that is absent in the classical simulations. However, in systems dominated by ionic interactions, the intermolecular structure may not be primarily dictated by the comparatively weaker hydrogen bonds. A liberal geometric definition of hydrogen bonds yields 10 such bonds per cation in the pure liquid versus 7 present in the crystal.⁷⁴ A conservative estimate is 1 hydrogen bond per cation in the liquid. The distribution of dipole moment components and magnitudes of the ions show that they are polarized significantly in the liquid environment compared to their electronic structure in the gas phase.²⁰

Previous AIMD simulations on [mmim][Cl] by Lynden-Bell and co-workers⁴⁸ using 8 and 24 ion pairs showed negligible system size effects. Their results were qualitatively similar to the results obtained from a 32 ion pair CPMD simulation performed by us.⁵⁰ In view of these, despite the rather small number of ion pairs employed in the current study, we believe that the intermolecular structure in terms of nearest neighbor arrangement is unlikely to differ with increasing system size. However, our AIMD simulation trajectory is much shorter than the structural and stress relaxation times of neat [bmim][PF₆]. Hence, the results may have some memory of the initial configuration. Significant differences between AIMD and MD results have been observed in some of the crucial pair correlation functions. This points to the fact that the intermolecular structure in the AIMD simulation has relaxed to some extent from the initial configuration. In addition, the cation–anion structure obtained from the two independent AIMD simulations, one on pure [bmim][PF₆] and another on the mixture, are similar.

TABLE 3: Ensemble Average of the Instantaneous Total Dipole Moment and Its Components for the Anion and the Cation, As Obtained from Classical and CPMD Simulations of Pure [bmim][PF₆] and Structure-Optimized Isolated Ions

model/phase	ion	$\langle\mu_x\rangle$ (D)	$\langle\mu_y\rangle$ (D)	$\langle\mu_z\rangle$ (D)	$\langle \mu \rangle$ (D)
MD (liquid)	[PF ₆]	0.01 ± 0.19	0.00 ± 0.19	0.00 ± 0.19	0.31 ± 0.13
MD (liquid)	[bmim]	-0.25 ± 0.21	0.00 ± 0.67	2.01 ± 0.36	2.15 ± 0.35
CPMD (liquid)	[PF ₆]	0.07 ± 0.71	0.11 ± 0.65	0.02 ± 0.63	1.06 ± 0.48
CPMD (liquid)	[bmim]	-0.17 ± 0.48	0.02 ± 0.70	2.51 ± 0.57	2.65 ± 0.55
CPMD (isolated)	[PF ₆]	-0.01	0.00	0.00	0.01
CPMD (isolated)	[bmim]	-0.88	-1.44	2.42	2.95

So, although the AIMD trajectory is short compared to common MD trajectory lengths, the fact that the two AIMD simulations provide similar data on pair correlation functions makes these results believable. The butyl tails in [bmim][PF₆] can interact via van der Waals interactions, which may not be captured well within DFT. However, we believe that the intermolecular structure of ILs containing short alkyl chains are dominated mostly by electrostatics.

CO₂ molecules are found to be predominantly solvated by the anion rather than the cation. The most probable orientation of the CO₂ molecule is tangential to the PF₆ sphere, in agreement with previous classical MD simulations,⁴⁰ and seemingly contradicts the conclusions drawn from X-ray scattering experiments.⁴¹ The latter deduced that CO₂ molecules penetrate the octahedral voids of the anion. The most probable locations of CO₂ around an anion have been determined using SDFs to be the octahedral voids around the anion. Out of the eight such voids, on average, only four are occupied for a given anion. A weak interaction of the oxygen of the CO₂ molecule with the ring hydrogen H(C3) of the cation is also observed. To explain the solubility of CO₂ in [bmim][PF₆], Berne and co-workers⁴⁰ have argued the importance of voids present in the neat IL to accommodate the CO₂ molecules. Our ab initio MD data are insufficient in spatial and temporal extents to add support to this thesis. The current work, however, also points to the role that specific interactions such as the hydrogen bond between the CO₂ and the ring hydrogen H(C3) could play in the solubility of CO₂ in ionic liquids. This was alluded to by Maginn and co-workers³⁸ who found a marginal change in the Henry's constants upon substituting a methyl group in the place of the hydrogen. We also differ from the conclusions of the X-ray scattering experiments⁴¹ on the assignment of the 3.6 Å peak in the total *g*(*r*) in the [bmim][PF₆]-CO₂ mixture. We contend that this peak arises from CO₂-CO₂ pair distances rather than CO₂-anion neighbors. Although the intermolecular RDF obtained from CPMD simulation differs from the experimental data⁴¹ for the CO₂-[bmim][PF₆] mixture, we point out that they compare well for the pure [bmim][PF₆] system. In addition, the trend of changes in the RDF upon addition of CO₂ is reproduced in the simulation. Further work is necessary to resolve the minor differences between experiment and simulation in the presence (or absence) of oscillations in the RDF of the mixture.

CO₂ molecules, which are present near the anions or the ring hydrogen H(C3), are found to deviate farther from a linear geometry than the rest of their kind. The change in geometry arises due to Lewis acid-base (or electron donor-acceptor) interactions in the former case and the formation of a weak hydrogen bond in the latter. The fluorine atoms (Lewis bases) can donate a partial electronic charge to the carbon atom (Lewis acid) of CO₂. The deviation from a linear structure results in the lifting of degeneracy in the bending mode of CO₂, which agrees qualitatively with spectroscopic experiments.³⁶ Thus, our results point out that apart from ion-quadrupole interactions that are expected between the anion and CO₂ ion-induced dipole interactions could also be important.

Acknowledgment. The research reported here is partially supported by the Department of Science and Technology and the Council of Scientific and Industrial Research, Government of India. We thank Dr. Axel Kohlmeyer for providing the pseudopotential for the fluorine atom and Dr. M. Kanakubo for fruitful discussions. B.L.B. thanks the Council of Scientific and Industrial Research, India, for a research fellowship.

References and Notes

- (1) DeSimone, J. M.; Guan, Z.; Elsbernd, C. S. *Science* **1992**, 257, 945.
- (2) Clarke, M. J.; Harrison, K. L.; Johnston, K. P.; Howdle, S. M. *J. Am. Chem. Soc.* **1997**, 119, 6399.
- (3) Nagashima, K.; Lee, C. T., Jr.; Xu, B.; Johnston, K. P.; DeSimone, J. M.; Johnson, C. S., Jr. *J. Phys. Chem. B* **2003**, 107, 1962.
- (4) Chen, B.; Siepmann, J. I.; Klein, M. L. *J. Phys. Chem. B* **2001**, 105, 9840.
- (5) (a) Salaniwal, S.; Cui, S. T.; Cummings, P. T.; Cochran, H. D. *Langmuir* **1999**, 15, 5188. (b) Salaniwal, S.; Cui, S. T.; Cochran, H. D.; Cummings, P. T. *Langmuir* **2001**, 17, 1773.
- (6) Senapati, S.; Keiper, J. S.; DeSimone, J. M.; Wignall, G. D.; Melnichenko, Y. B.; Frielinghaus, H.; Berkowitz, M. L. *Langmuir* **2002**, 18, 7371.
- (7) Welton, T. *Chem. Rev.* **1999**, 99, 2071.
- (8) Earle, M. J.; Seddon, K. R. *Pure Appl. Chem.* **2000**, 72, 1391.
- (9) Triolo, A.; Mandanici, A.; Russina, O.; Rodriguez-Mora, V.; Cutroni, M.; Hardacre, C.; Nieuwenhuyzen, M.; Bleif, H.; Keller, L.; Ramos, M. A. *J. Phys. Chem. B* **2006**, 110, 21357.
- (10) Berg, R. W.; Deetlefs, M.; Seddon, K. R.; Shim, I.; Thompson, J. M. *J. Phys. Chem. B* **2005**, 109, 19018.
- (11) Hanke, C. G.; Price, S. L.; Lynden-Bell, R. M. *Mol. Phys.* **2001**, 99, 801.
- (12) Hanke, C. G.; Atamas, N. A.; Lynden-Bell, R. M. *Green Chem.* **2002**, 4, 107.
- (13) Lynden-Bell, R. M.; Atamas, N. A.; Vasilyuk, A.; Hanke, C. G. *Mol. Phys.* **2002**, 100, 3225.
- (14) Lynden-Bell, R. M. *Mol. Phys.* **2003**, 101, 2625.
- (15) Del-Popolo, M. G.; Voth, G. A. *J. Phys. Chem. B* **2004**, 108, 1744.
- (16) Lynden-Bell, R. M.; Kohanoff, J.; Del Popolo, M. G. *Faraday Discuss.* **2005**, 129, 57-6.
- (17) Hu, Z.; Margulis, C. J. *Proc. Natl. Acad. Sci. U.S.A.* **2006**, 103, 831.
- (18) Yan, T.; Li, S.; Jiang, W.; Gao, X.; Xiang, B.; Voth, G. A. *J. Phys. Chem. B* **2006**, 110, 1800.
- (19) Karmakar, R.; Samanta, A. *J. Phys. Chem. A* **2003**, 107, 7340.
- (20) Yan, T.; Burnham, C. J.; Del Popolo, M. G.; Voth, G. A. *J. Phys. Chem. B* **2004**, 108, 11877.
- (21) Wang, Y.; Voth, G. A. *J. Am. Chem. Soc.* **2005**, 127, 12192.
- (22) Tsuzuki, S.; Tokuda, H.; Hayamizu, K.; Watanabe, M. *J. Phys. Chem. B* **2005**, 109, 16474.
- (23) Hunt, P. A. *Mol. Simul.* **2006**, 32, 1.
- (24) Koßmann, S.; Thar, J.; Kirchner, B.; Hunt, P. A.; Welton, T. *J. Chem. Phys.* **2006**, 124, 174506.
- (25) Hunt, P. A.; Kirchner, B.; Welton, T. *Chem.-Eur. J.* **2006**, 12, 6762.
- (26) Hunt, P. A.; Gould, I. R. *J. Phys. Chem. A* **2006**, 110, 2269.
- (27) Bhargava, B. L.; Balasubramanian, S. *J. Chem. Phys.* **2005**, 123, 144505.
- (28) Gong, L.; Guo, W.; Xiong, J.; Li, R.; Wu, X.; Li, W. *Chem. Phys. Lett.* **2006**, 425, 167.
- (29) Wang, Y.; Li, H.; Han, S. *J. Chem. Phys.* **2006**, 124, 044504.
- (30) (a) Watterscheid, P. *Nature* **2006**, 439, 797. (b) Earle, M. J.; Esperanca, J. M. S. S.; Gilea, M. A.; Lopes, J. N. C.; Rebelo, L. P. N.; Magee, J. W.; Seddon, K. R.; Widegren, J. A. *Nature* **2006**, 439, 831.
- (31) Blanchard, L. A.; Hancu, D.; Beckman, E. J.; Brennecke, J. F. *Nature* **1999**, 399, 28.
- (32) Cole-Hamilton, D. J. *Science* **2003**, 299, 1702.
- (33) Scurto, A. M.; Aki, S. N. V. K.; Brennecke, J. F. *J. Am. Chem. Soc.* **2002**, 124, 10276.
- (34) Scurto, A. M.; Leitner, W. *Chem. Commun.* **2006**, 3681.
- (35) Fletcher, K. A.; Baker, S. N.; Baker, G. A.; Pandey, S. *New J. Chem.* **2003**, 27, 1706.
- (36) Kazarian, S. G.; Briscoe, B. J.; Welton, T. *Chem. Commun.* **2000**, 2047.
- (37) Lu, J.; Liotta, C. L.; Eckert, C. A. *J. Phys. Chem. A* **2003**, 107, 3995.
- (38) Cadena, C.; Anthony, J. L.; Shah, J. K.; Morrow, T. I.; Brennecke, J. F.; Maginn, E. J. *J. Am. Chem. Soc.* **2004**, 126, 5300.
- (39) Deschamps, J.; Costa Gomes, M. F.; Pádua, A. A. H. *ChemPhysChem* **2004**, 5, 1049.
- (40) Huang, X.; Margulis, C. J.; Li, Y.; Berne, B. J. *J. Am. Chem. Soc.* **2005**, 127, 17842.
- (41) Kanakubo, M.; Umecky, T.; Hiejima, Y.; Aizawa, T.; Nanjo, H.; Kameda, Y. *J. Phys. Chem. B* **2005**, 109, 13847.
- (42) Kroon, M. C.; Karakatsani, E. K.; Economou, I. G.; Witkamp, G.; Peters, C. J. *J. Phys. Chem. B* **2006**, 110, 9262.
- (43) Blanchard, L. A.; Gu, Z.; Brennecke, J. F. *J. Phys. Chem. B* **2001**, 105, 2437.
- (44) Anthony, J. L.; Maginn, E. J.; Brennecke, J. F. *J. Phys. Chem. B* **2002**, 106, 7315.

- (45) Kamps, A. P.; Tuma, D.; Xia, J.; Maurer, G. *J. Chem. Eng. Data* **2003**, *48*, 746.
- (46) Husson-Borg, P.; Majer, V.; CostaGomes, M. F. *J. Chem. Eng. Data* **2003**, *48*, 480.
- (47) Anthony, J. L.; Anderson, J. L.; Maginn, E. J.; Brennecke, J. F. *J. Phys. Chem. B* **2005**, *109*, 6366.
- (48) Del Pópolo, M. G.; Lynden-Bell, R. M.; Kohanoff, J. *J. Phys. Chem. B* **2005**, *109*, 5895.
- (49) Bühl, M.; Chaumont, A.; Schurhammer, R.; Wipff, G. *J. Phys. Chem. B* **2005**, *109*, 18591.
- (50) Bhargava, B. L.; Balasubramanian, S. *Chem. Phys. Lett.* **2006**, *417*, 486.
- (51) Raugei, S.; Klein, M. L. *ChemPhysChem* **2004**, *5*, 1569.
- (52) Boero, M.; Ikeshoji, T.; Liew, C. C.; Terakura, K.; Parrinello, M. *J. Am. Chem. Soc.* **2004**, *126*, 6280.
- (53) Kirchner, B.; Seitsonen, A. P.; Hutter, J. *J. Phys. Chem. B* **2006**, *110*, 11475.
- (54) Morrone, J. A.; Haslinger, K. E.; Tuckerman, M. E. *J. Phys. Chem. B* **2006**, *110*, 3712.
- (55) Aki, S. N. V. K.; Mellein, B. R.; Saurer, E. M.; Brennecke, J. F. *J. Phys. Chem. B* **2004**, *108*, 20355.
- (56) The solubility data for CO₂ in [bmim][PF₆] obtained from ref 55 were fitted to a second-order polynomial, which yielded the volume expansion to be 1.312 for the 70 mol % (CO₂) mixture of [bmim][PF₆]-CO₂ relative to pure [bmim][PF₆]. A value of 1.30 was chosen to arrive at the simulation density that agrees with the value that is used in ref 41.
- (57) Car, R.; Parrinello, M. *Phys. Rev. Lett.* **1985**, *55*, 2471.
- (58) Hutter, J.; Ballone, P.; Bernasconi, M.; Focher, P.; Foïs, E.; Goedecker, S.; Marx, D.; Parrinello, M.; Tuckerman, M. E. *CPMD*, version 3.11.1; Max Planck Institut fuer Festkoerperforschung, Stuttgart, Germany, and IBM Zurich Research Laboratory: 1990–2006.
- (59) Troullier, N.; Martins, J. L. *Phys. Rev. B* **1991**, *43*, 1993.
- (60) Becke, A. D. *Phys. Rev. A* **1988**, *38*, 3098.
- (61) Lee, C.; Yang, W.; Parr, R. G. *Phys. Rev. B* **1988**, *37*, 785.
- (62) Martyna, G. J.; Klein, M. L.; Tuckerman, M. E. *J. Chem. Phys.* **1992**, *97*, 2635.
- (63) Harris, J. G.; Yung, K. H. *J. Phys. Chem.* **1995**, *99*, 12021.
- (64) (a) Lopes, J. N. C.; Deschamps, J.; Pádua, A. A. H. *J. Phys. Chem. B* **2004**, *108*, 2038. (b) Lopes, J. N. C.; Deschamps, J.; Pádua, A. A. H. *J. Phys. Chem. B* **2004**, *108*, 11250.
- (65) Borodin, O.; Smith, G. D.; Jaffe, R. L. *J. Comput. Chem.* **2001**, *22*, 641.
- (66) Bhargava, B. L.; Balasubramanian, S. *J. Am. Chem. Soc.* **2006**, *128*, 10073.
- (67) Tuckerman, M. E.; Berne, B. J.; Martyna, G. *J. Chem. Phys.* **1992**, *97*, 1990.
- (68) Wannier, G. H. *Phys. Rev.* **1937**, *52*, 191.
- (69) Boys, S. F. *Rev. Mod. Phys.* **1960**, *32*, 296.
- (70) Resta, R. *Rev. Mod. Phys.* **1994**, *66*, 899.
- (71) Resta, R.; Sorella, S. *Phys. Rev. Lett.* **1999**, *82*, 370.
- (72) Berghold, G.; Mundy, C. J.; Romero, A. H.; Hutter, J.; Parrinello, M. *Phys. Rev. B* **2000**, *61*, 10040.
- (73) Resende Prado, C. E.; Del Pópolo, M. G.; Youngs, T. G. A.; Kohanoff, J.; Lynden-Bell, R. M. *Mol. Phys.* **2006**, *104*, 2477.
- (74) (a) Choudhury, A. R.; Winterton, N.; Steiner, A.; Cooper, A. I.; Johnson, K. A. *J. Am. Chem. Soc.* **2005**, *127*, 16792. (b) Dibrov, S. M.; Kochi, J. K. *Acta Crystallogr., Sect. C: Cryst. Struct. Commun.* **2006**, *62*, o19.
- (75) Guzei, I. A.; Langenhan, J. M. *Acta Crystallogr., Sect. C: Cryst. Struct. Commun.* **2003**, *59*, i95.
- (76) *CRC Handbook of Chemistry and Physics*, 81st ed. Lide, D. R., Ed.; CRC Press: Boca Raton, FL, 2000; Chapter 9, p 20.
- (77) Madden, P. A.; Wilson, M. *Chem. Soc. Rev.* **1996**, *25*, 339.
- (78) Margulis, C. J.; Stern, H. A.; Berne, B. J. *J. Phys. Chem. B* **2002**, *106*, 12017.
- (79) Morrow, T. I.; Maginn, E. J. *J. Phys. Chem. B* **2002**, *106*, 12807.
- (80) Liu, Z.; Huang, S.; Wang, W. *J. Phys. Chem. B* **2004**, *108*, 12978.
- (81) Urahata, S. M.; Ribeiro, M. C. C. *J. Chem. Phys.* **2004**, *120*, 1855.
- (82) *Crystal Design: Structure and Function*; Desiraju, G. R. Ed.; Perspectives in Supramolecular Chemistry 7; Wiley: Chichester, U. K., 2004; p 6.
- (83) Kokalj, A. *J. Mol. Graphics Modell.* **1999**, *17*, 176.
- (84) Hardacre, C.; Holbrey, J. D.; McMath, S. E. J.; Bowron, D. T.; Soper, A. K. *J. Chem. Phys.* **2003**, *118*, 273.
- (85) Dong, K.; Zhang, S.; Wang, D.; Yao, X. *J. Phys. Chem. A* **2006**, *110*, 9775.
- (86) Tong, G. S. M.; Cheung, A. S. C. *J. Phys. Chem. A* **2002**, *106*, 11637.
- (87) Saharay, M.; Balasubramanian, S. *J. Chem. Phys.* **2004**, *120*, 9694.
- (88) Yan, T.; Burnham, C. J.; Del Pópolo, M. G.; Voth, G. A. *J. Phys. Chem. B* **2004**, *108*, 11877.
- (89) (a) Sloutskin, E.; Ocko, B. M.; Tamam, L.; Kuzmenko, I.; Gog, T.; Deutsch, M. *J. Am. Chem. Soc.* **2005**, *127*, 7796. (b) Sloutskin, E.; Ocko, B. M.; Tamam, L.; Kuzmenko, I.; Gog, T.; Deutsch, M. *J. Am. Chem. Soc.* **2005**, *127*, 18333.
- (90) Balasubramanian, S.; Bhargava B. L. Unpublished work.